Measurement of the Branching Ratio of the CP-Violating Decay Mode $K_L^0 \to 2\pi^0$

I. A. Budagov,* D. C. Cundy, G. Myatt, F. A. Nezrick,† G. H. Trilling,‡ W. Venus, and H. Yoshiki

CERN, Geneva, Switzerland

AND

B. Aubert, P. Heusse, I. Le Dong, J. P. Lowys, D. Morellet, E. Nagy,|| and C. Pascaud

Laboratoire de l'Accélérateur Linéaire, Faculté des Sciences, Orsay, France

AND

L. Behr, P. Beillière, G. Boutang, and M. Schiff

Ecole Polytechnique, Paris, France

(Received 30 March 1970)

The branching ratio $\Gamma(K_L^0 \to 2\pi^0)/\Gamma(K_L^0 \to 3\pi^0)$ has been measured directly, using a heavy-liquid bubble chamber, and found to be $(3.2\pm1.5)\times10^{-3}$, from which $|\eta_{00}| = (1.9\pm0.5)\times10^{-3}$.

I. INTRODUCTION

FOLLOWING the discovery[1] of the CP-violating decay mode $K_L^0 \to \pi^+\pi^-$, the present experiment at the CERN proton synchrotron was designed to look for the corresponding neutral mode $K_L^0 \to \pi^0\pi^0$ and to measure its branching ratio. Comparison of the rates of these two modes allows in principle the elimination of certain hypotheses as to the origin of the CP-violating effect. Preliminary results from this experiment have been reported previously.[2]

The basic idea of the experiment was to pass a K_L^0 beam through a large heavy-liquid bubble chamber, observe the disintegrations $K_L^0 \to 2\pi^0$ and $K_L^0 \to 3\pi^0$ (both giving rise only to γ rays), and thus determine directly the ratio of the rates

$$R = \Gamma(K_L^0 \to 2\pi^0)/\Gamma(K_L^0 \to 3\pi^0).$$

* Now at Laboratory of Nuclear Problems, Joint Institute for Nuclear Research, Dubna, USSR.

† Now at National Accelerator Laboratory, Batavia, Ill.

‡ National Science Foundation Senior Postdoctoral Fellow. Permanent address: Lawrence Radiation Laboratory, University of California, Berkeley, Calif.

|| Present address: Central Research Institute of Physics, Budapest, Hungary.

[1] J. M. Christenson, J. W. Cronin, V. L. Fitch, and R. Turlay, Phys. Rev. Letters **13**, 138 (1964).

[2] I. A. Budagov, D. C. Cundy, G. Myatt, F. A. Nezrick, G. H. Trilling, W. Venus, H. Yoshiki, B. Aubert, P. Heusse, I. Le Dong, J. P. Lowys, D. Morellet, E. Nagy, C. Pascaud, L. Behr, P. Beillière, G. Boutang, M. Schiff, and J. Van der Velde, Phys. Letters **28B**, 215 (1968); in Proceedings of the Topical Conference on Weak Interactions, CERN Report No. 69-7, 1969, p. 298 (unpublished).

To avoid background from regenerated K_S^0, the K_L^0 beam was very sharply collimated and transported through the center of the chamber inside an evacuated pipe. The bubble chamber was filled with heavy freon (CF_3Br) in order to maximize the γ-detection efficiency; it was thus essentially a 4π detector of γ rays from K_L^0 decays occurring in the fiducial region of the beam pipe. Its high spatial resolving power allowed the efficient detection and measurement even of γ rays of low energy emitted at large angles. It also allowed precise error estimates to be made for all the measured variables; a systematic and extensive study was carried out in order to confirm their precision and reliability. This made possible the use of sophisticated kinematic fitting techniques to distinguish $K_L^0 \to 2\pi^0$ events from the background of $K_L^0 \to 3\pi^0$ events with only four visible γ rays. This was the only important background in the experiment. It was studied by Monte Carlo techniques. These were tested with the aid of measured $K_L^0 \to 3\pi^0$ events with six visible γ rays, any two of which could be thrown away in order to simulate a background event.

In Sec. II we describe experimental details such as the disposition of the beam and bubble chamber, the scanning, selection, measurement and kinematical fitting procedures, the checks made on the precision and reliability of the measurements, and the method used to study the background to the $K_L^0 \to 2\pi^0$ mode coming from $3\pi^0$ decays. Section III then presents the estimation of the over-all detection efficiency for $K_L^0 \to 2\pi^0$

events, and two kinematical analyses of the $2\pi^0$ candidates, one based on kinematical fits to the $2\pi^0$ hypothesis in which the mass of the parent particle is considered unknown, and one in which it is fixed at the mass of the K_L^0 and the $3\pi^0$ hypothesis is also considered. Our conclusions are summarized in Sec. IV.

II. EXPERIMENTAL TECHNIQUES

A. K_L^0 Beam

1. Layout of Beam

The beam line consisted essentially of three 3-m-long collimators, each followed by a charged-particle sweeping magnet (see Fig. 1). It accepted neutral particles emitted at 30° to the circulating 19.2-GeV/c proton beam direction. The beryllium target was 2 mm in diameter and 50 mm long, with its axis on the K_L^0 beam axis. About 7×10^{10} protons were used per burst, giving about 50 K_L^0, 700 γ rays above 1 GeV, and 3500 neutrons above 300 MeV at the bubble chamber.[3]

The beam was completely defined by the target and collimator C2, producing a 2-cm-diam beam at the bubble chamber. The solid angle accepted was 4.5×10^{-7} sr and the angular divergence ± 0.4 mrad. C1 reduced the flux of particles on the front of C2, while C3 absorbed particles scattered off the inside of C2. The holes through the collimators were tapered towards the target. Each collimator consisted of a 3-m-long brass tube, 30 mm in diameter, filled with appropriately predrilled brass cylinders and held in a cylindrical slot machined between two large steel blocks.

A Monte Carlo program simulating the absorption and scattering of beam particles was used to design the collimator system in detail. It predicted that only one K_L^0 would pass through the bubble chamber outside the

vacuum pipe during the entire exposure of 5×10^5 pictures, provided that the collimators were precisely aligned. This was done with the aid of a telescope, stationed behind the bubble chamber, with which one could look along the whole beam line to the target. Illuminated Lucite cones installed at each end of each collimator could, when required, be positioned with their apexes accurately on the collimator axis. The collimators were then adjusted until their cones fell on the beam line. The bubble chamber was aligned using two cross-hairs inside the vacuum pipe. Finally, the target position was adjusted until the beam profile, measured just behind the bubble chamber, was symmetric about the optical beam axis.

The air pressure inside the beam pipe through the bubble chamber was reduced to 4×10^{-2} mm Hg. This "vacuum" region extended continuously for 14 m from window W2 in front of collimator C2. Outside the bubble chamber, when not limited by collimators, the vacuum region was 180 mm in diameter. Inside the bubble chamber it was 40 mm in diameter.

2. Measured Beam Size

The shape of the beam profile was determined frequently during the exposure by scanning with a finger counter of dimensions $1 \times 1 \times 100$ mm mounted parallel to the beam, just behind the bubble chamber. A typical result is shown in Fig. 2. The shape thus determined was essentially that of the neutron component in the beam.

To check that the shape of the K_L^0 component was essentially the same, the decay points of some 300 $K_L^0 \rightarrow \pi^+\pi^-\pi^0$ events were determined by geometrical reconstruction and kinematic fitting. For other decay modes, the reconstruction errors were larger. All the
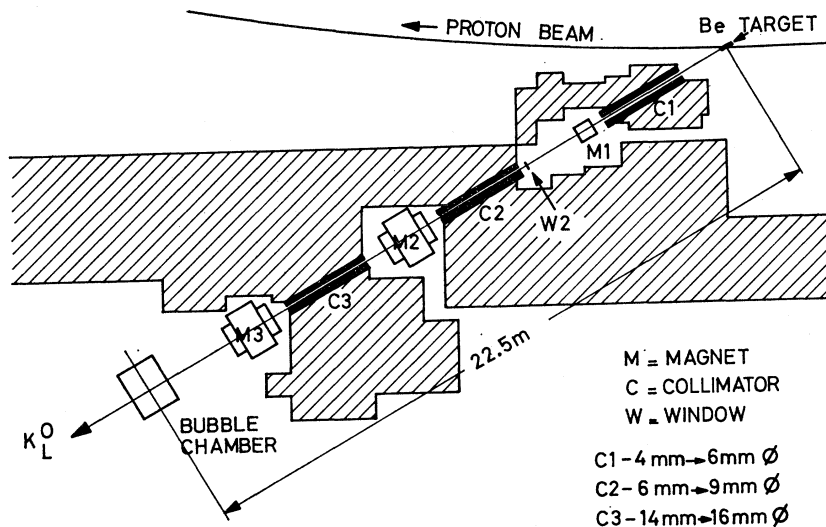

FIG. 1. Experimental layout.

M = MAGNET
C = COLLIMATOR
W = WINDOW

C1 - 4 mm → 6 mm ∅
C2 - 6 mm → 9 mm ∅
C3 - 14 mm → 16 mm ∅

[3] H. J. Gerber, G. Fisher, R. Jones, and A. Wattenberg, Illinois Internal Report No. ILL 39, 1962 (unpublished).

measured K_L^0 beam profiles were consistent with expectations based on the counter measurements, the reconstruction errors, and the assumption that the neutron and K_L^0 profiles were identical. These measurements also allowed the beam direction relative to the bubble-chamber coordinate system to be determined within ±1.8 mrad.

However, these beam-profile measurements are not sensitive enough to the possible presence of a small tail extending outside the beam pipe. Even a few K_L^0 entering the liquid or pipe wall during the exposure could produce a significant background consisting of $2\pi^0$ decays of regenerated K_S^0. On the assumption that any such K_L^0 would be accompanied by neutrons in roughly the same proportion as in the main beam, the order of magnitude of this K_L^0 flux was estimated from the corresponding neutron flux. A special scan for proton recoils was performed using 12 500 pictures selected so as to sample the entire exposure. It was calculated that for each proton recoil observed in this scan, roughly 0.05 $2\pi^0$ events due to regenerated K_S^0 should have been seen in the scan for $2\pi^0$ events.

The total of 287 proton recoils observed should thus have corresponded to about 14 $K_S^0 \rightarrow 2\pi^0$ decays distributed widely throughout the chamber liquid, and in fact some seven such candidates were observed. However, only two recoils were observed within 5 cm of the beam pipe. This corresponds to a negligible background of only 0.05 $K_S^0 \rightarrow 2\pi^0$ decays occurring in the whole of the $2\pi^0$ experiment in the near vicinity of the fiducial volume used.

3. K_L^0 Momentum Distribution

The K_L^0 momentum distribution was determined by measurement and kinematic fitting of $K_L^0 \rightarrow \pi^+\pi^-\pi^0$ events with two γ rays converted in the chamber. The error in the fitted K_L^0 momentum was typically about ±6%.

The observed momentum distribution $\Phi_{obs}(p)$ has to be corrected for detection inefficiencies in order to obtain the real momentum distribution $\Phi_{ch}(p)$ of K_L^0 mesons decaying in the chamber. The corrections were applied by weighting the individual events. They did not substantially change the shape of the momentum distribution, as can be seen from Fig. 3.

B. Bubble Chamber

The CERN heavy-liquid bubble chamber used for this experiment is cylindrical in shape, 1.2 m in diameter, and 1 m deep. It was filled with heavy freon CF_3Br (radiation length 11 cm). The magnetic field was 27 kG.

The beam passed through the bubble chamber, in a direction perpendicular to the axis of the chamber and the magnetic field and at a depth of 60 cm below the front glass, inside an evacuated aluminium pipe of
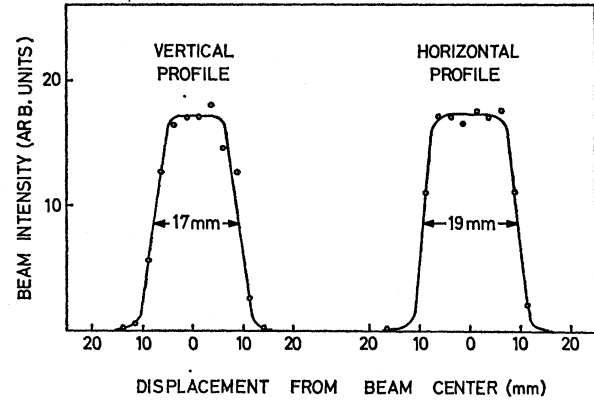

FIG. 2. Profile of the neutron component accompanying the K_L^0 beam, measured with a 1×1-mm finger counter just behind the bubble chamber.

inside diameter 4 cm and wall thickness 2.5 mm. A large lead cylinder, 20 cm in diameter and 10 cm long, was clamped around the upstream end of the beam pipe in order to reduce the flux into the chamber of secondaries of K_L^0 decays occurring further upstream.

A long plane mirror, suspended freely in the liquid from the back plate of the chamber, allowed the cameras to photograph the region behind the pipe. The mirror was situated at a depth of 95 cm below the front glass. Fiducial crosses were painted along the back of the beam pipe. Measurement of their apparent positions, as
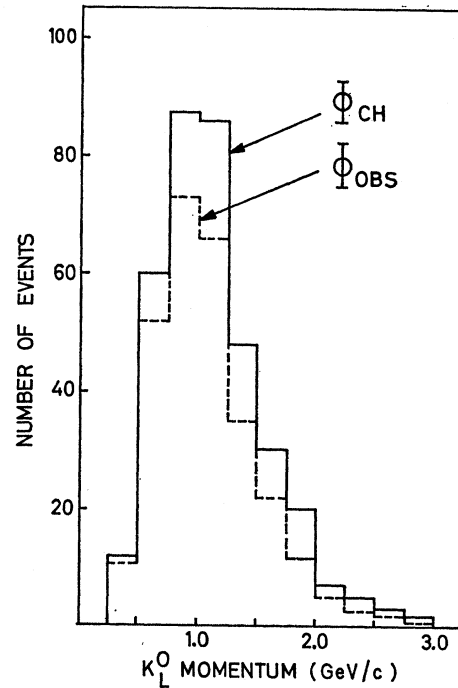

FIG. 3. Momentum distribution of the K_L^0 particles decaying in the fiducial region. Φ_{obs} is the distribution directly observed. Φ_{ch} is that obtained after correcting for losses.

seen in the mirror, determined the instantaneous position and orientation of the mirror in each photograph and also the slight instantaneous flexing produced as it swung through the liquid. The geometrical reconstruction programs took this flexing into account in the reconstruction of points and tracks measured with the aid of the mirror.

C. Scanning and Event Selection

All possible decays of $K_L{}^0$ into any number of γ rays and no charged secondaries ("$n\gamma$ events") were noted unless either (a) the intersection point of the γ rays was clearly outside the 50-cm-long fiducial region, or (b) the photograph was "illegal" because of the presence of additional events, the secondaries of which might be confused with those of the $n\gamma$ event. Any photograph containing two $n\gamma$ events with $n \geq 3$ was "illegal," as was any photograph in which a charged track not due to an electron emerged from the beam pipe either within 15 cm of the γ intersection point (criterion A) or within the fiducial volume extended by 15 cm in the downstream direction (criterion B). About half of the $n\gamma$ events were found by using each criterion (Table I). Events due to the $2\pi^0$ and $3\pi^0$ decay modes were thus picked up simultaneously in the scanning, avoiding a possible source of bias.

At the scanning stage, all visible γ rays that pointed close to the $K_L{}^0$ decay point were noted and classified as either "ambiguous" or "sure," according to whether or not another possible origin besides the $K_L{}^0$ decay point could be seen. More than 99% of the "ambiguous" γ rays were classified in this way because they were possibly bremsstrahlung of another γ ray originating in the same event.

Subsequently, all $n\gamma$ events recorded by the scanners were inspected by physicists, who checked their legality, modified, if necessary, the classification of γ's as "sure" or "ambiguous," and searched for additional γ's. All events that could possibly be interpreted as containing four primary γ rays (i.e., $n_{\text{sure}} \leq 4 \leq n_{\text{sure}} + n_{\text{ambiguous}}$) were so interpreted. These "4γ candidates" were then measured.

As a result of the exclusion of "illegal" photographs, less than 1% of $n\gamma$ events contained either seven "sure" primary γ's or an "ambiguous" γ whose alternative origin was unrelated to the $n\gamma$ event. Thus the number of 4γ candidates containing an accidentally associated

γ ray originating in a different event was negligible; and so was the number of 4γ events rejected as 5γ events because of such γ's.

D. Measurement Procedures

Measurements were made using image-plane digitizers with a least count of $100\,\mu$ and a space-to-image demagnification of 1.7. The geometrical reconstruction programs used were modified versions of JONAS[4] at Orsay and at the Ecole Polytechnique, and of DRAT[5] at CERN. Empirical correction factors were included in both programs to allow for optical distortions in the cameras and projectors, and to improve the precision of reconstruction. The allowance for the slight flexing of the mirror was handled differently in the two programs. In JONAS, the mirror was assumed to be spherical. Its parameters were determined by simultaneously fitting all the measurements of the beam-pipe fiducial marks in the photograph. The radius of curvature was typically found to be ~ 100 m. In DRAT, a more general mirror distortion was allowed for by determining the local orientation of each region of the mirror from the measurements of only the nearest fiducial mark images. The consistency of the two programs was checked by reconstructing a sample of events with both programs.

Three different techniques were used to determine the momenta and directions of the γ rays: the Behr-Mittner (BM) method[6] was used at the Ecole Polytechnique and at CERN, and supplemented at CERN by use of the total-track-length (TTL) method,[7,8] while the SPIGAM method[9] was used at Orsay.

In the BM method, electrons are measured either up to the nearest kink or point of visible bremsstrahlung emission, or up to an optimum length depending on the radius of curvature and determined using a template. A helix is then fitted to the reconstructed light rays. The initial momentum and direction thus determined are then corrected, using the calculated average rate of momentum loss by ionization and "invisible" bremsstrahlung emission. The errors are determined from the average measurement errors and the calculated effects of multiple scattering and fluctuations in invisible bremsstrahlung loss. The γ energy is taken as the sum of the electron energies and its direction as the weighted average of their directions.

A bremsstrahlung carrying away much of the electron energy may be emitted so near to the γ conversion point that the initial electron energy cannot be measured, only its final energy. In such cases we measured both the

TABLE I. Summary of scanning results.

Scan results	Scan criterion A	Scan criterion B	Total
No. of photos scanned	125 000	275 000	400 000
5γ or 6γ events	6 700	7 200	13 900
4γ candidates	1 700	1 400	3 100
Total $n\gamma$ events ($n \geq 2$)	8 500	8 700	17 200

[4] B. Jacquet, D. Morellet, and J. Six, Orsay and Ecole Polytechnique groups (private communication).
[5] K. Soop, CERN Internal Report No. NPA/Int. 66-13, 1966 (unpublished).
[6] L. Behr and P. Mittner, Nucl. Instr. Methods 20, 446 (1963).
[7] B. Eiben, CERN Internal Report No. NPA/Int. 66-6, 1966 (unpublished).
[8] R. Arnold, I. A. Budagov, F. A. Nezrick, and W. A. Venus, CERN Internal Report No. NPA/Int. 68-9, 1968 (unpublished).
[9] D. Morellet, Orsay Internal Report No. LAL 1190, 1968 (unpublished).

electron pair produced directly and the pair produced by the bremsstrahlung, and added their energies together. This reduces both the correction for invisible bremsstrahlung loss and the associated statistical error.

The SPIGAM method is essentially a refinement of the BM method in which the spiralization of the electron tracks is taken into account directly by fitting a spiral (i.e., a helix of steadily decreasing radius of curvature) rather than a simple helix. The scattering and bremsstrahlung errors are taken into account directly in the fit, as well as the measurement errors. The two electron tracks are fitted simultaneously using the constraint that their initial directions are the same. Fewer electrons are rejected by this method as being "unmeasurable" than are rejected by the BM method.

In the TTL method, which determines only the γ energy but not its direction, the magnetic field is not used. Instead, the bubble chamber is used as a total ionization calorimeter, the measured quantity being the total length of all electron tracks associated with the electromagnetic cascade initiated by the γ. The relationship between the total track length and the γ energy depends also on the potential length available in the chamber for the development of the shower, and on the smallest soft-photon energy that can be seen and unambiguously associated with the shower. This relationship, and also the errors on the energy values obtained, were determined[8] for our experimental conditions by applying the method to γ's coming from $K_L{}^0 \rightarrow \pi^+\pi^-\pi^0$ decay whose energies were already known to better than $\pm 10\%$ from the results of a kinematic fit. The energy values obtained with the TTL and BM methods are practically independent, and were combined to increase the precision.

E. Checks of Measurement Procedures

1. Reconstruction Using Mirror

Some γ conversion points close to the side of the beam pipe could be measured both with and without use of the mirror. A sample of such vertices were measured both

ways and the results were compared. Small systematic shifts (smaller than the error in measuring a single point) were observed between the directly reconstructed and the mirror-reconstructed positions. However, distorting the x, y, and z coordinates of γ vertices in Monte Carlo $2\pi^0$ events by corresponding amounts was found to have a negligible effect on the results of kinematic fits to the $2\pi^0$ hypothesis, the errors in x, y, and z being typically negligible compared with the γ-direction errors.

This conclusion was supported by the observation that in $\pi^+\pi^-\pi^0$ decays measured and fitted to the hypothesis $K_L{}^0 \rightarrow \pi^+\pi^-\pi^0$ with free $K_L{}^0$ mass, the $K_L{}^0$ mass distribution obtained from events containing at least one track measured in the mirror was indistinguishable from that obtained from events containing no such track.

2. γ-Direction Measurements

Several checks of the correctness of γ-direction measurements were made. For measured γ's contained in 4γ candidates, a comparison was made between the measured directions of the electron and positron in the same pair. The observed direction difference divided by the calculated error in the direction difference should ideally be a Gaussian of unit variance, and in fact approximated this very closely. In addition, a sample of neutral pions produced in interactions of charged pions in the chamber liquid were measured. In these events, the true γ directions were known rather precisely from the positions of the production and conversion points, and could be compared with their measured directions (the point reconstruction errors being, as already mentioned, typically negligible compared with the γ-direction errors). Figure 4 shows this comparison. Finally, Fig. 5 shows the χ^2 probability distribution for a purely geometrical 5C fit in which the gammas in 4γ candidates were constrained to come from a common origin. Provided the direction errors are correctly estimated, the distribution should be flat.
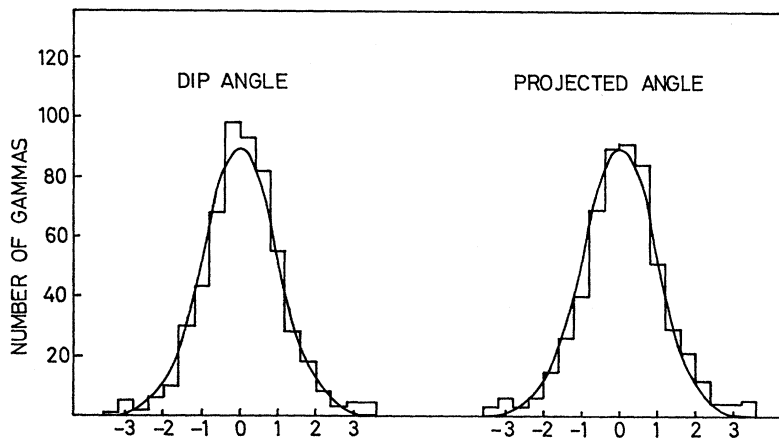

FIG. 4. Difference in (i) dip angle δ and (ii) projected angle ϕ between the known and measured directions of γ rays produced in visible interactions in the chamber liquid, in units of the calculated error in the difference. The curves show the distributions expected if the errors are correctly calculated, namely, Gaussians of unit variance.
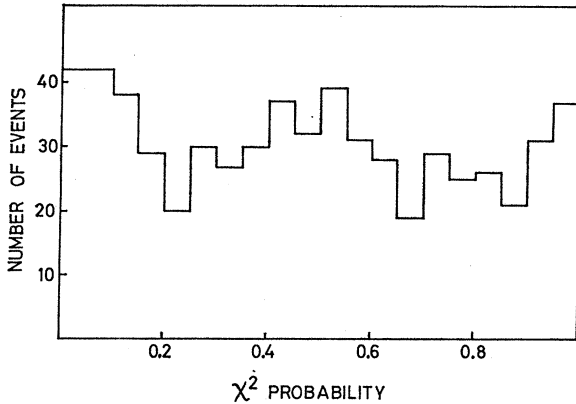
FIG. 5. χ^2 probability distribution for a geometrical 5C fit constraining the γ rays to a common origin, applied to 4γ candidates.

3. γ-Energy Measurements

The γ-energy measurement procedures applied to the 4γ candidates were checked by applying them also to the measurement of the π^0 and K_L^0 masses. The neutral pions used came partly from the interactions of charged pions in the liquid and partly from $K_L^0 \rightarrow \pi^+\pi^-\pi^0$ decays. The K_L^0 mass was measured using $K_L^0 \rightarrow 3\pi^0$ decays with six converted γ rays.

The mass was calculated using

$$m = [(\sum_i E_i)^2 - (\sum_i \mathbf{p}_i)^2]^{1/2}.$$

Any systematic bias in the γ-energy values would bias the average observed mass by the same factor. Since the γ-conversion-point and γ-direction errors are relatively unimportant, the widths of the mass distributions reflect directly the true errors in the γ energies. The mass
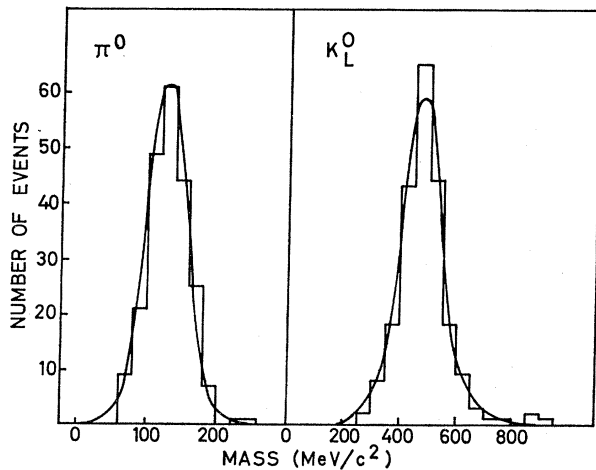

FIG. 6. Observed π^0 and K_L^0 mass distributions obtained by measuring $\pi^0 \rightarrow 2\gamma$ and $K_L \rightarrow 3\pi^0 \rightarrow 6\gamma$ events with the techniques used to measure the 4γ candidates. The curves show the widths expected.
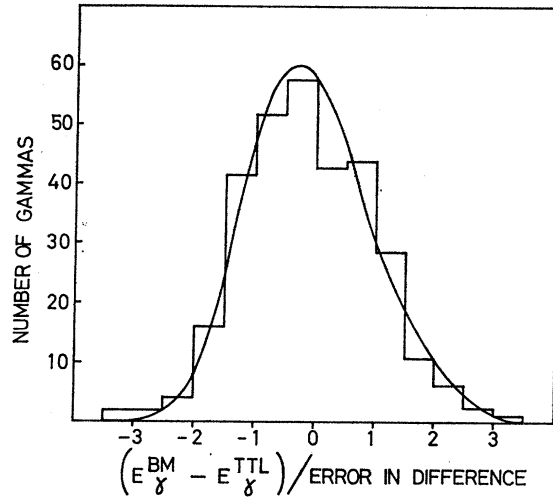

FIG. 7. Difference between TTL and BM energy values, for γ rays in 4γ candidates, in units of the error in the difference. The solid curve shows the distribution expected.

distributions observed are shown in Fig. 6, where the curves show the widths expected on the basis of the assigned measurement errors.

A direct check of the energy measurements made on the 4γ candidates themselves could be made for those γ's measured by both the BM and TTL methods. Figure 7 shows the observed distribution of the difference between the two energy values for each such γ, divided by the quadratic sum of the two errors. The curve shown is the distribution expected if the errors are Gaussian in E_γ^{TTL} and in $1/E_\gamma^{\mathrm{BM}}$.

4. Measurement Precision

In all three laboratories, the rather exhaustive checks made on the reliability and precision of the measurements thus established the absence of any significant bias in either the measured values or the errors assigned to them. Except for the relatively unimportant errors in reconstructing the positions of the γ conversion points, these errors were dominated by the contributions from multiple Coulomb scattering and bremsstrahlung emission. Typical values of the calculated errors are given in Table II.

TABLE II. Typical measurement errors.

Measured parameter	Typical error
x, y of conversion point	±0.2 mm
z of conversion point	±2.0 mm
Dip angle of γ	$240/(E_{\mathrm{MeV}})^{0.8}$ deg
Azimuthal angle of γ	$115/(E_{\mathrm{MeV}})^{0.8}$ deg
γ energy (BM)	24%
γ energy (SPIGAM)	23%
γ energy (TTL)	20%
γ energy (BM+TTL)	17%

F. Kinematic Analysis

Once a sample of 4γ events has been measured, the kinematic analysis should allow the separation of those coming from $K_L^0 \to 2\pi^0$ decays from those from $K_L^0 \to 3\pi^0$ decays. The principles of the kinematic analysis procedures used are outlined in Sec. II F 1. In order to determine their efficiency, to check that the $2\pi^0$ events could indeed be separated, and to study the behavior of the $3\pi^0$ background in the region of the $2\pi^0$ signal, 4γ events from both $2\pi^0$ and $3\pi^0$ decays were generated by a Monte Carlo method (Sec. II F 2) and treated by these procedures. The background is of great importance in our case since the signal is small. Therefore, $K_L^0 \to 3\pi^0 \to 4\gamma$ events were also generated by withdrawing two γ's at a time from a measured sample of $K_L^0 \to 3\pi^0 \to 6\gamma$ events (Sec. II F 3), and these were used to check the reliability of the Monte Carlo calculations.

1. Kinematic Fitting Procedure

For each event, one can make the following hypotheses:

$$K_L^0 \to \pi^0 + \pi^0$$
$$\searrow \quad \searrow \qquad (j=1)$$
$$2\gamma \quad 2\gamma$$

$$\to \pi^0 + \pi^0 + \pi^0$$
$$\searrow \quad \searrow \quad \searrow \qquad (j=2)$$
$$2\gamma \quad 2\gamma \quad 0\gamma$$

$$\to \pi^0 + \pi^0 + \pi^0$$
$$\searrow \quad \searrow \quad \searrow \qquad (j=3).$$
$$2\gamma \quad 1\gamma \quad 1\gamma$$

Furthermore, for each hypothesis there are several possible ways of pairing the γ's: three for $j=1$ and $j=2$, and six for $j=3$. Thus for each event we can make the 12 hypotheses H_{jk}, where the index k denotes the pairing. Our kinematic fitting procedure gives the likelihood ratios of the various competing hypotheses,[10] in the manner outlined below.

Assuming any given one of these hypotheses H_{jk}, let us compute the likelihood of having obtained for an event the N measured values x_μ^m for the conversion points of the γ's, their directions, and their momenta, given the initial K_L^0 direction. Let J be the number of constraint equations between the x_μ. Then the decay may be described by $N-J$ independent variables which we call θ_i. For $j=1$ $(K_L^0 \to 2\pi^0)$, for example, the θ_i may conveniently be chosen as the K_L^0 momentum and decay-point coordinates, two angles in the K_L^0 center-of-mass system, two angles in each of the π^0 rest frames, and the four conversion lengths of the γ's.

The true values x_μ corresponding to the measured values x_μ^m can be expressed as functions of the inde-

pendent variables θ_i. Let us define, for this hypothesis,

$$\chi^2(\theta_i) = [x_\mu(\theta_i) - x_\mu^m] g_{\mu\nu} [x_\nu(\theta_i) - x_\nu^m],$$

where $g^{-1}{}_{\mu\nu}$ is the error matrix. The probability of obtaining the measured values x_μ^m, given the θ_i, is then

$$\frac{(|g_{\mu\nu}|)^{1/2}}{(2\pi)^{N/2}} e^{-\chi^2(\theta_i)/2} \prod_\mu dx_\mu^m.$$

The over-all likelihood of obtaining the x_μ^m, given the hypothesis, is obtained by multiplying by $p(\theta_i)\prod_i d\theta_i$, the *a priori* probability of the decay occurring with values θ_i, and integrating over all θ_i:

$$\mathcal{L}(x_\mu^m) = \frac{(|g_{\mu\nu}|)^{1/2}}{(2\pi)^{N/2}} \int e^{-\chi^2(\theta_i)/2} p(\theta_i) \prod_i d\theta_i.$$

Since contributions to the integral come only from θ_i near θ_i^f, this integral may be approximated by[10,11]

$$\mathcal{L}(x_\mu^m) = \frac{1}{(2\pi)^{J/2}} e^{-[\chi^2(\theta_i^f) - 2\ln p(\theta_i^f)]/2} \left(\frac{|g_{\mu\nu}|}{|d_{lm}|}\right)^{1/2},$$

where the θ_i^f are the "fitted" values of θ_i which minimize the quantity

$$\chi'^2(\theta_i) = \chi^2(\theta_i) - 2\ln p(\theta_i),$$

and

$$d_{lm} = \frac{\partial x_\mu}{\partial \theta_l} g_{\mu\nu} \frac{\partial x_\nu}{\partial \theta_m} - \frac{\partial^2}{\partial \theta_l \partial \theta_m}[\ln p(\theta_i)] \quad \text{for} \quad \theta_i = \theta_i^f.$$

One can thus compute the likelihood $\mathcal{L}(x_\mu^m)$ of each hypothesis provided one can find the values of the θ_i which minimize χ'^2.

To do this, we write

$$\frac{\partial \chi'^2}{\partial \theta_i} = \frac{\partial x_\mu}{\partial \theta_i} g_{\mu\nu}(x_\nu - x_\nu^m) - \frac{2}{p} \frac{\partial p}{\partial \theta_i} = 0$$

and solve this set of $N-J$ equations with $N-J$ unknowns θ_i by linearization and iteration. In the fitting procedure used, for example, in GRIND, the variables fitted are the measured ones x_μ which can be set equal to their measured values x_μ^m for the first iteration. However, there is no such evident set of starting values for the θ_i. Starting values were obtained either from simplified "GRIND-like" fits in which the γ directions were assumed to be known precisely, or by repeatedly choosing random sets of θ_i until one was found with an initial value of χ'^2 small enough to begin the iteration process.

The likelihoods $\mathcal{L}(x_\mu^m)$ thus calculated present two important advantages over the classical χ^2 probabilities. First, they use more information, namely, our knowledge of the *a priori* distribution of the θ_i. Second, the

---

[10] L. Behr, Thèse de doctorat d'Etat, Paris, Série A 4515, No. 5362, 1965 (unpublished).

[11] C. Pascaud, Thèse de doctorat d'Etat, Paris, Orsay, Série A, No. 233, 1967 (unpublished); Orsay Internal Report No. LAL 1171, 1967 (unpublished).

likelihoods $\mathcal{L}_{jk}$ of the competing hypotheses H_{jk} can be compared directly and used, as in Sec. III C, in an over-all maximum-likelihood fit.

In highly constrained fits, such as for hypotheses $j=1$, most of the information comes from comparison of the measurements with the constraints and relatively little from the *a priori* distributions of the θ_i. The first kinematical analysis given below in Sec. III B employs only fits to hypotheses $j=1$ and no over-all maximum-likelihood fit. Thus it is essentially unaltered by use of this procedure, rather than the classical one of minimizing χ^2 instead of χ'^2 and calculating the χ^2 probability.

In weakly constrained fits, on the other hand, the added information is often critically important. In particular, in an unconstrained or underconstrained fit, as occurs for hypotheses $j=3$, it allows the likelihood $\mathcal{L}_{jk}$ to be determined even though the classical χ^2 probability is undefined. However, the approximation used above in evaluating the integral over all θ_i is then a very rough one. The kinematic "residues" observed in the second analysis given in Sec. III C are probably mainly due to use of this approximation.

2. Generation of Monte Carlo Events

Both $K_L{}^0 \rightarrow 2\pi^0$ and $K_L{}^0 \rightarrow 3\pi^0$ events were generated. The exact chamber geometry and the variation of the average γ conversion length with γ energy were both taken into account. Events in which four γ's converted in the chamber were then selected, and the conversion-point coordinates, directions, and energies of the γ's were distorted according to the known measurement errors.

The variables chosen at random in the generation of the events were the θ_i defined above. Their *a priori* distribution $p(\theta_i)$ was known from (i) experimental study of $K_L{}^0 \rightarrow \pi^+\pi^-\pi^0$ decays for the $K_L{}^0$ momentum and decay-point coordinates, and (ii) from physical laws, such as the isotropy of γ emission in the π^0 rest frame, for the other variables. The x_μ were then computed from the θ_i and distorted according to Gaussian error distributions.

Since not all γ's are equally well measured, the sizes of the measurement errors to be assigned had first to be chosen. Two methods were used. In the first, the laws of the distribution and behavior of the measurement-error sizes were determined empirically from the measured events, and the errors were chosen accordingly. In the second, a list of measured γ's was constructed and each generated γ was assigned the errors of the one having the nearest values of momentum, emission angle, dip angle, potential length for shower development, etc. This method automatically takes into account the actual distribution and behavior of the measurement error sizes.

Samples of 500 $K_L{}^0 \rightarrow 2\pi^0$ and 15 000 $K_L{}^0 \rightarrow 3\pi^0$ decays were generated by both methods.

3. Check of Monte Carlo Procedure for Background Determination

A sample of 4γ events closely resembling the background to the $K_L{}^0 \rightarrow 2\pi^0$ signal can be generated by measuring $K_L{}^0 \rightarrow 3\pi^0$ events with six converted γ's and discarding two of the γ's. These events were not used to evaluate the background directly, since the relative frequencies of different configurations are not the same as in the background and weight factors would therefore have to be introduced, resulting in large statistical errors. Instead, the Monte Carlo procedures used to predict the behavior of the background were verified by checking that they correctly predicted the behavior of these events.

Two independent samples of such events were studied. The first consisted of 1200 4γ events generated from 80 6γ events by removing all possible combinations of two γ's in turn. However, the strong correlations between the 15 4γ events generated from the same 6γ event entail a large statistical error. In the second sample, therefore, only one 4γ event was generated from each of another sample of 1067 6γ events. This event was selected at random from among the 15 possible ones according to their relative probabilities of being observed as 4γ events. These 4γ events were subjected to the kinematical analyses used to separate the $K_L{}^0 \rightarrow 2\pi^0$ events.

Monte Carlo $K_L{}^0 \rightarrow 3\pi^0$ events with six converted γ's were then generated and treated in the same way. The results were compared and found to be in good agreement (e.g., see Fig. 10 below).

III. ANALYSIS

A. Determination of Detection Efficiencies

1. γ-Ray Detection Efficiency

The average γ detection efficiency was determined experimentally in two ways. The value obtained from the relative numbers of $K_L{}^0 \rightarrow \pi^+\pi^-\pi^0$ decays observed as $\pi^+\pi^-$ 1γ and $\pi^+\pi^-$ 2γ events was $(89\pm1)\%$. That obtained from the fraction of $K_L{}^0 \rightarrow 3\pi^0$ decays observed as 2γ, 3γ, or 4γ events, after correcting for the small observed numbers of $K_L{}^0 \rightarrow 2\pi^0$ and $K_L{}^0 \rightarrow 2\gamma$ [12] events, was $(88\pm2)\%$.

These results were compared with the predictions of Monte Carlo calculations in which the exact chamber geometry was used, the variation of conversion length with γ energy according to the Bethe-Heitler formula was taken into account, as was the Compton scattering cross section, and the momentum distribution of the decaying $K_L{}^0$ particles was assumed to be that shown in Fig. 5 (Φ_{ch}). With these assumptions, the γ conversion efficiency was predicted to be 95%.

[12] R. Arnold, I. A. Budagov, D. C. Cundy, G. Myatt, F. Nezrick, G. H. Trilling, W. Venus, H. Yoshiki, B. Aubert, P. Heusse, E. Nagy, and C. Pascaud, Phys. Letters **28B**, 56 (1968).

Various parametrizations of the extra loss of γ rays, depending on the γ energy and the location of its conversion point in the chamber, were tried. For each one, the parameters were adjusted so as to fit the efficiencies observed for the $\pi^+\pi^-\pi^0$ and $3\pi^0$ decay modes. These parametrizations were then introduced into the Monte Carlo generation of $K_L^0 \rightarrow 2\pi^0$ decays, and the probability of converting and seeing all four γ's was recalculated.

γ rays from all decay modes have the same angular distribution, and the change in average conversion length due to the change in average γ energy is not large. Consequently, the results did not depend strongly on the mechanism assumed for the extra loss of γ's. We concluded from these studies that the probability of converting and seeing all four γ rays from a $K_L^0 \rightarrow 2\pi^0$ decay was $(65\pm5)\%$.

2. Bremsstrahlung Cut

All events that could possibly be interpreted as 4γ candidates were accepted and measured as $K_L^0 \rightarrow 2\pi^0$ candidates. Thus many 5γ events were accepted because two of the γ's were approximately aligned so that it was feasible, at the scanning table, to interpret one as being bremsstrahlung of the other. And some 3γ events were accepted because one of the γ's gave rise to a bremsstrahlung that pointed close to the K_L^0 decay point. A simple bremsstrahlung cut was therefore applied after measurement to remove many of these 5γ and 3γ events.

Two γ's were considered "aligned" when the angle α between (i) the line of flight from the reconstructed K_L^0 decay point to the nearer γ conversion point, and (ii) the line from that conversion point to the second one, was less than 300 mrad. When two of the possible primary γ's were "aligned," the second was considered to be bremsstrahlung of the first; otherwise, both were considered to be primary. Those 4γ candidates containing either three or five primary γ's according to this criterion were rejected.

Some of the real $2\pi^0$ events were falsely rejected as 3γ events by this cut because of the alignment of two primaries. By applying the cut to Monte Carlo $2\pi^0$ events, this fraction was found to be $(4\pm1)\%$. Some others were falsely rejected as 5γ events because of the presence of a bremsstrahlung pointing close to the K^0 decay point but lying outside the 300-mrad cone. By applying the cut to the measured 6γ events, this loss was found to be $(4\pm2)\%$. The total loss of real $2\pi^0$ events was therefore $(8\pm2)\%$.

Of the total number of 4γ candidates, 32% were rejected by this cut; 11% of these were rejected as 3γ events, in agreement with the Monte Carlo prediction for 4γ events resulting predominantly from $K_L^0 \rightarrow 3\pi^0$ decays. Of the remaining 21% rejected as 5γ events, some 4% were rejected falsely because of a brems-

strahlung lying outside the cone and therefore $(17\pm2)\%$ were in fact 5γ events.

The 4γ candidates were compared with a sample of events containing six clearly primary γ's in which all the "bremsstrahlungs" were therefore genuine. The differences between the observed distributions in α and r (where α is the angle defined above to which the bremsstrahlung cut was applied, and r is the ratio of the energy of the bremsstrahlung to the energy remaining in the electron pair) indicated that some 35% of all the 4γ candidates were actually 5γ events. Thus about half of the 5γ events remained after this cut.

3. Scanning and Selection Efficiency

The $2\pi^0$ and $3\pi^0$ events were picked up simultaneously in the scanning. In a rescan of 30% of the film, no difference was observed between the scanning efficiencies for 4γ candidates and other $n\gamma$ events. This scanning efficiency, which cancels out in the measured ratio, was found to be 88%.

The $2\pi^0$ events are contained among the 4γ candidates that satisfy the scanning rules and pass the bremsstrahlung cut. The reproducibility with which such events were picked out from the $n\gamma$ events was found to be $(73\pm11)\%$ by repeating independently the selection of 4γ candidates from 30% of the film.

A large fraction of the events that were selected only once were ambiguous between the 4γ and 5γ classifications, because they contained an energetic γ that could have been either bremsstrahlung or primary. The comparisons already mentioned between the 4γ candidates and the clear 6γ events indicated that these were mostly 5γ events. The above figure is thus an underestimate of the selection efficiency for true 4γ events.

Taking into account the uncertainty in correcting for the presence of 5γ events and that in extrapolating from true 4γ events in general to those from $2\pi^0$ decay, we estimate that the selection efficiency for 4γ events from $2\pi^0$ decays was $(80\pm15)\%$.

4. Event Measurability

The largest class of unmeasurable events consists of events in which one or more γ rays converted in the aluminum wall of the beam pipe. Since 4% of γ's were classified as "pipe" γ's at the scanning and event-selection stages, this class contained 16% of the $2\pi^0$ events. In another 4% of events, although measurements were made, it was not possible to achieve sufficiently complete geometrical reconstruction.

5. Over-All Detection Efficiency

The over-all efficiency for detecting and measuring a $K_L^0 \rightarrow 2\pi^0$ decay is therefore the product of the following factors: (a) probability of converting and seeing all four γ rays in the chamber ($=0.65\pm0.05$), (b) probability of selecting the events as a 4γ candidate ($=0.80\pm0.15$),

(c) probability of it being measurable ($=0.80\pm0.02$), and (d) probability of it passing the bremsstrahlung cut ($=0.92\pm0.02$). This efficiency is equal to 0.38 ± 0.08.

B. Kinematic Analysis Using Fits to $K_L^0 \to 2\pi^0$ Hypotheses with Variable K_L^0 Mass

Kinematic fits were made to the hypotheses $K_L^0 \to 2\pi^0 \to 4\gamma$ (hypotheses $j=1$ in Sec. II F 1) treating the mass of the K_L^0 as one of the independent unknown variables θ_i. Genuine $K_L^0 \to 2\pi^0 \to 4\gamma$ events then yield mass values narrowly distributed about the true K_L^0 mass. Background events, $K_L^0 \to 3\pi^0$ with four visible γ's, typically yield lower mass values.

Figure 8 shows the mass distribution obtained with the following conditions, designed to reduce the background as much as possible without significantly reducing the signal.

(a) Of the three possible ways of pairing the γ's in each event, only the pairing that yields the highest likelihood $\mathcal{L}_{1k}$ (see Sec. II F 1) is considered. Study of Monte Carlo events indicated that in 96% of true $K_L^0 \to 2\pi^0$ events, $\mathcal{L}_{1k}$ is larger for the true pairing than for either of the false pairings.

(b) The corresponding χ^2 probability is required to be $\geq 10\%$.

(c) The fitted K_L^0 momentum is required to lie in the range $0.4 < p_K < 2.0$ GeV/c. Most of the decaying K_L^0
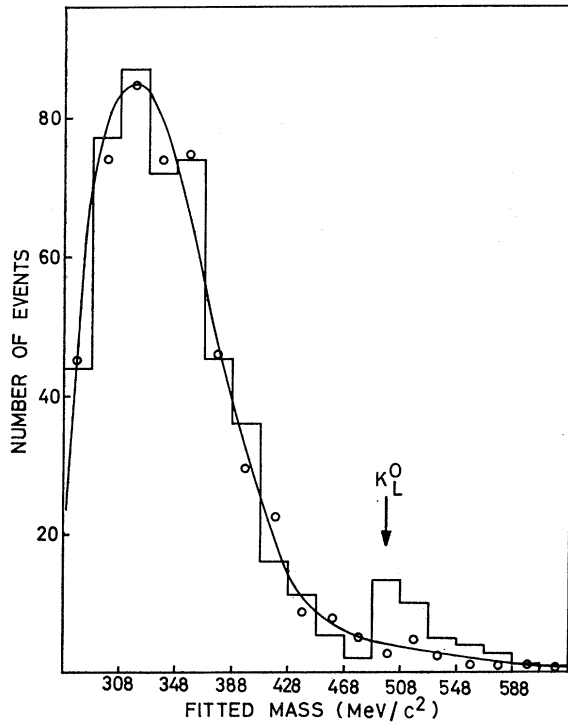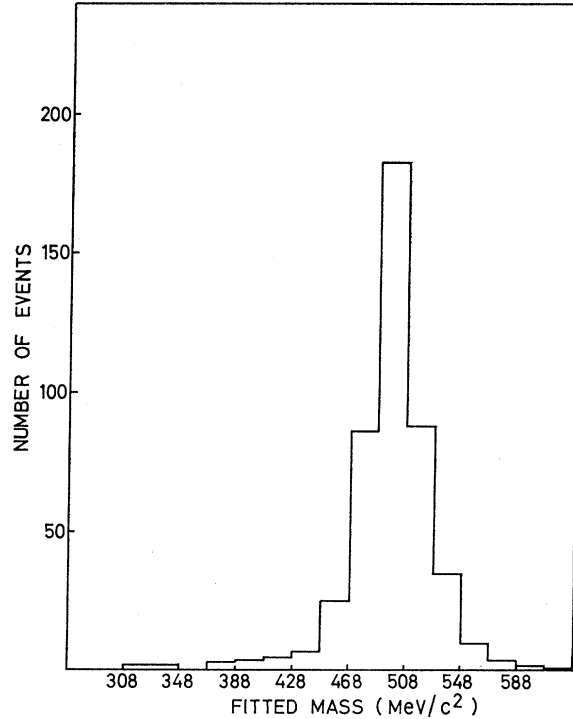
FIG. 9. Fitted mass distribution of Monte Carlo $K_L^0 \to 2\pi^0 \to 4\gamma$ events.

have momenta in this range (Fig. 3). In background events, two of the γ's are missing and the lower visible energy biases the fitted p_K distribution to lower values. On the other hand, if one of the γ energies was unmeasurable, a fit may be found in which this γ, and therefore the K_L^0, is assigned a very high momentum. Consequently, rejection of fits with very high and very low values of p_K improves the signal-to-noise ratio.

With these conditions, there are 30 events inside the fiducial region in the fitted mass range $468 < m_K < 548$ MeV/c^2. The mass range is chosen to be asymmetric about the K_L^0 mass because the background is much higher on the low-mass side.

Figure 9 shows the corresponding mass distribution obtained by the same procedure from a sample of 541 Monte Carlo $K_L^0 \to 2\pi^0 \to 4\gamma$ events. Of these, 85 events were rejected by the above cuts and a further 65 yielded fitted mass values outside the required range. The probability of a measured $K_L^0 \to 2\pi^0 \to 4\gamma$ event yielding a mass value in the range $468 < m_K < 548$ MeV/c^2 and satisfying the above conditions is thus found to be $(72\pm3)\%$.

The curve in Fig. 8 shows the background predicted by applying the same procedure to 3500 Monte Carlo $K_L^0 \to 3\pi^0 \to 4\gamma$ events. The curve is normalized to the number of events in the histogram. Outside the K_L^0 mass region, the shape of the fitted mass distribution is predicted correctly.[13] In the K_L^0 mass region, there is a

FIG. 8. Fitted mass distribution of observed 4γ candidates (histogram) and predicted background (points and curve).

clear excess of events due to $K_L{}^0 \rightarrow 2\pi^0 \rightarrow 4\gamma$ decays. Figure 10 shows the good agreement, in the same conditions, between the 4γ events generated from real 6γ events and the corresponding Monte Carlo predictions[13] (see Sec. II F 3); it thus verifies the reliability of the background prediction.

The background predicted among the 30 events with $468 < M < 548$ MeV/c^2 is 15 ± 3 events, where the quoted error reflects the precision with which the Monte Carlo predictions have been verified. Thus 15 ± 6 events are due to $K_L{}^0 \rightarrow 2\pi^0$ decay. The over-all detection efficiency of $2\pi^0$ events is the product of the efficiency for detecting and measuring a $K_L{}^0 \rightarrow 2\pi^0$ decay [0.38 ± 0.08 (see Sec. III A 5)] and the above probability of it then yielding a mass value in the required range under the above conditions (0.72 ± 0.03). From these figures and the total number of $n\gamma$ events (17 150), we find the branching ratio to be

$$R = \Gamma(K_L{}^0 \rightarrow 2\pi^0)/\Gamma(K_L{}^0 \rightarrow 3\pi^0) = (3.2 \pm 1.5) \times 10^{-3}.$$

The difference between this result and the preliminary result previously quoted,[2] which was based on a similar analysis, is due mainly to a reevaluation of the background.
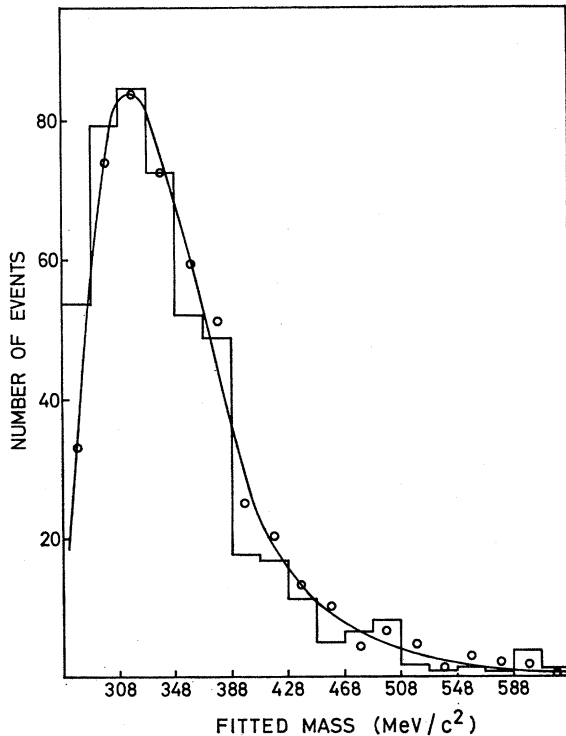

FIG. 10. Fitted mass distributions of artificial $K_L{}^0 \rightarrow 3\pi^0 \rightarrow 4\gamma$ events generated by rejecting γ rays two at a time from (i) measured 6γ events (histogram) and (ii) Monte Carlo 6γ events (points and curve).

---

[13] If the Monte Carlo curve is instead normalized to the number of events entering the fits, the number of events in the histogram is also predicted correctly within 10%.

C. Kinematic Analysis Using Fits to All $K_L{}^0 \rightarrow 2\pi^0$ and $K_L{}^0 \rightarrow 3\pi^0$ Hypotheses with Fixed $K_L{}^0$ Mass

The preceding analysis is based on fits to the hypotheses $K_L{}^0 \rightarrow 2\pi^0 \rightarrow 4\gamma$ ($j = 1$) only. In principle, the background in the $K_L{}^0$ mass region can be distinguished from the signal by also making fits to the hypotheses $K_L{}^0 \rightarrow 3\pi^0 \rightarrow 4\gamma$ ($j = 2$ and $j = 3$). Background events should typically yield a good fit to one or other of these hypotheses, while true $K_L{}^0 \rightarrow 2\pi^0 \rightarrow 4\gamma$ events should not. Therefore, in this second analysis, new fits to all 12 possible hypotheses (see Sec. II F 1) were made with the $K_L{}^0$ mass fixed at its true value, and the likelihoods $\mathcal{L}_{jk}$ of the different hypotheses were compared.

The value of α,

$$\alpha = \frac{\Gamma(K_L{}^0 \rightarrow 2\pi^0)}{\Gamma(K_L{}^0 \rightarrow 2\pi^0) + \Gamma(K_L{}^0 \rightarrow 3\pi^0)},$$

was then extracted directly from the total data by maximizing the following log-likelihood function:

$$\mathcal{L}(\alpha) = N^{2\gamma} \ln[\alpha p_2{}^{2\gamma} + (1-\alpha) p_3{}^{2\gamma}]$$
$$+ N^{3\gamma} \ln[\alpha p_2{}^{3\gamma} + (1-\alpha) p_3{}^{3\gamma}]$$
$$+ (N^{5\gamma} + N^{6\gamma}) \ln[(1-\alpha)(p_3{}^{5\gamma} + p_3{}^{6\gamma})]$$
$$+ \sum_{4\gamma \text{ events}} \ln[\alpha p_2{}^{4\gamma} \pi_2 + (1-\alpha) p_3{}^{4\gamma} \pi_3],$$

where $p_{2(3)}{}^{n\gamma}$ is the probability of a $2(3)\pi^0$ event being observed with n γ's, $N^{n\gamma}$ is the observed number of events with n γ's,

$$\pi_2 = \tfrac{1}{3} \sum_{k=1,3} \mathcal{L}_{1k}$$

and

$$\pi_3 = \tfrac{1}{9} \left(\sum_{k=1,3} \mathcal{L}_{2k} + \sum_{k=1,6} \mathcal{L}_{3k} \right).$$

The sum over 4γ events is the most important term in the expression for $\mathcal{L}(\alpha)$. It takes account of the kinematic fit results through the values of $\mathcal{L}_{jk}$. The term in $N^{5\gamma} + N^{6\gamma}$ appears only for normalization. The terms in $N^{2\gamma}$ and $N^{3\gamma}$ have only a small influence on α by comparing the observed and expected numbers of 2γ and 3γ events. The contribution from $n < 2$ has been neglected.

The uncorrected value of α obtained by this maximum-likelihood method from 70% of the data, taking into account the detection and measurement efficiency for $2\pi^0$ events (Sec. III A), was $\alpha = (7.7 \pm 1.5) \times 10^{-3}$.

A pure sample of $3\pi^0$ decays should, in principle, yield a value of α compatible with zero. In fact it does not, because of kinematics inefficiency. If the fit corresponding to the correct hypothesis fails to converge, the corresponding $\mathcal{L}_{jk}$ value will be zero, π_3 will be underestimated, and the final estimate of α will be too large. In addition, as noted in Sec. II F 1, the expression used to calculate the values of $\mathcal{L}_{jk}$ is only a rough approximation in the case of hypotheses $j = 3$. This background

("residue") due to $3\pi^0$ events, which is of computational order only, was evaluated by applying the method to Monte Carlo $3\pi^0$ events and found to be $\alpha_r = (4.4 \pm 1.7) \times 10^{-3}$. Subtracting this from the uncorrected value of α, we find

$$\alpha = (3.3 \pm 2.2) \times 10^{-3}.$$

Conversely, and for similar reasons, a pure sample of $2\pi^0$ decays does not yield $\alpha = 1$. However, application of the method to a sample of Monte Carlo $2\pi^0$ events yielded $\alpha = 0.98 \pm 0.02$, indicating that the loss of $2\pi^0$ events is negligible and that no further correction is necessary.

The above figure, based on 70% of the data, is in agreement with that obtained from the preceding analysis using all the data, $\alpha = (3.2 \pm 1.5) \times 10^{-3}$.

IV. SUMMARY AND CONCLUSIONS

The mass distribution (Fig. 8) obtained by fitting the 4γ events to the hypothesis $K_L^0 \to 2\pi^0$ with variable K_L^0 mass shows a peak at the true K_L^0 mass value. This peak is well separated from the background distribution due to $K_L^0 \to 3\pi^0$ decays with two undetected γ rays. It constitutes clear evidence of the existence of the neutral CP-violating decay mode $K_L^0 \to 2\pi^0$. The branching ratio $R = \Gamma(K_L^0 \to 2\pi^0)/\Gamma(K_L^0 \to 3\pi^0)$ deduced from this distribution has been compared with that obtained from a more sophisticated maximum-likelihood fit to 70% of the total data. In this, each 4γ event is fitted not only to the $K_L^0 \to 2\pi^0$ hypothesis (with fixed K_L^0 mass) but also to the alternative $K_L^0 \to 3\pi^0$ hypothesis, and the relative likelihood of the two hypotheses is evaluated. The results of the two analyses are in agreement. We conclude that

$$R = \Gamma(K_L^0 \to 2\pi^0)/\Gamma(K_L^0 \to 3\pi^0) = (3.2 \pm 1.5) \times 10^{-3}.$$

Using the following values[14]:

$$\frac{\Gamma(K_L^0 \to \pi^0\pi^0\pi^0)}{\Gamma(K_L^0 \to \text{charged modes})} = 0.275 \pm 0.011,$$

$$\tau_{K_L^0} = (5.4 \pm 0.2) \times 10^{-8} \text{ sec},$$

$$\tau_{K_S^0} = (8.62 \pm 0.06) \times 10^{-11} \text{ sec},$$

$$\frac{\Gamma(K_S^0 \to 2\pi^0)}{\Gamma(K_S^0 \to \text{all modes})} = 0.313 \pm 0.006,$$

we find $|\eta_{00}|^2 = (3.5 \pm 1.7) \times 10^{-6}$, where the quoted errors include systematic as well as statistical errors.

The numerous internal consistency checks that have been made during the course of the experiment give confidence in the results. Particular care was taken to check the correctness of the estimated measurement

---

TABLE III. Measured values of $|\eta_{00}|^2$.

$10^3 R$	$10^6|\eta_{00}|^2$	Reference
3.2 ± 1.5	3.5 ± 1.7	this expt
4.6 ± 1.1	5.1 ± 1.2	15
13.1 ± 3.1	14.1 ± 3.4	16
(regenerator)	-2.0 ± 7.0	17
(regenerator)	13.0 ± 4.0	18
(regenerator)	10.2 ± 4.5	19

errors, of critical importance for the reliability of the kinematic fit results; and also to check the Monte Carlo predictions of the behavior of the $K_L^0 \to 3\pi^0$ background with the aid of measured 6γ events, from which background 4γ events could be generated artificially by ignoring two of the γ's.

Our result may be compared with others already published. These may be divided into (i) those in which the branching ratio R is measured and $|\eta_{00}|^2$ deduced, and (ii) those in which a regenerator is used and $|\eta_{00}|^2$ is measured directly. The results are summarized in Table III.

The values of $|\eta_{00}|^2$ are so widely dispersed that there is apparently little sense in averaging them. It is clear that the $K_L^0 \to 2\pi^0$ mode exists. The crucial question is whether or not $|\eta_{00}|^2 = |\eta_{+-}|^2 = (3.6 \pm 0.2) \times 10^{-6}$, as required by the simplest ("superweak") model of CP violation yet proposed. This prediction is well verified by the result of the present experiment.

In the phenomenological description of $K_L^0 \to 2\pi$ decays based on CPT invariance, $|\eta_{00}|$ can be related to other measured parameters $|\eta_{+-}|$, Φ_{+-}, Φ_{00}, and Reϵ, the values of which are given in Table IV. A fit to these data using the well-known relationships $\eta_{+-} = \epsilon + \epsilon'$ and

TABLE IV. Values of other CP-violation parameters (from Ref. 20).

Parameter	"Superweak" prediction	Measured value
$|\eta_{+-}|$		$(1.90 \pm 0.05) \times 10^{-3}$
Φ_{+-}	$43° \pm 1°$	$39.8° \pm 6.0°$
Reϵ	$(1.39 \pm 0.05) \times 10^{-3}$	$(1.42 \pm 0.17) \times 10^{-3}$
Φ_{00}	$43° \pm 1°$	$17.0° \pm 31.0°$

[14] Taken from the data compilation of A. Barbaro-Galtieri, S. E. Derenzo, L. R. Price, A. Rittenberg, A. H. Rosenfeld, N. Barash-Schmidt, C. Bricman, M. Roos, P. Söding, and C. G. Wohl, Rev. Mod. Phys. **42**, 87 (1970).

[15] M. Banner, J. W. Cronin, J. K. Liu, and J. E. Pilcher, Phys. Rev. Letters **21**, 1107 (1968); Phys. Rev. **188**, 2033 (1969).

[16] R. J. Cence, B. D. Jones, V. Z. Peterson, V. J. Stenger, J. Wilson, R. D. Eandi, R. W. Kenney, I. Linscott, W. P. Oliver, S. Parker, and C. Rey, Phys. Rev. Letters **22**, 1210 (1969).

[17] D. F. Bartlett, R. K. Carnegie, V. L. Fitch, K. Goulianos, D. P. Hutchinson, T. Kamae, R. F. Roth, J. S. Russ, and W. Vernon, Phys. Rev. Letters **21**, 558 (1968).

[18] J. M. Gaillard, W. Galbraith, A. Hussri, M. R. Jane, N. H. Lipman, G. Manning, T. J. Ratcliffe, H. Faissner, and H. Reithler, in *Proceedings of the Fourteenth International Conference on High-Energy Physics, Vienna, 1968* (CERN, Geneva, 1968); Nuovo Cimento **59A**, 453 (1969).

[19] J. Chollet, J. M. Gaillard, M. R. Jane, T. J. Ratcliffe, J. P. Repellin, K. R. Schubert, and B. Wolff, in Proceedings of the Topical Conference on Weak Interactions, CERN Report No. 69-7, 1969, p. 309 (unpublished).

[20] Taken from the review by J. Steinberger, in Proceedings of the Topical Conference on Weak Interactions, CERN Report No. 69-7, 1969, p. 291 (unpublished).

$\eta_{00} = \epsilon - 2\epsilon'$ yields $|\eta_{00}| = (1.4_{-0.7}^{+1.2}) \times 10^{-3}$ if the phase of ϵ is left free, or $|\eta_{00}| = (2.0 \pm 0.7) \times 10^{-3}$ if it is constrained to equal $43° \pm 1°$ as predicted by most models. Our result, $|\eta_{00}| = (1.9 \pm 0.5) \times 10^{-3}$, is clearly compatible with these predictions.

ACKNOWLEDGMENTS

Reaction $\pi^+ p \rightarrow p\pi^+\pi^+\pi^-\pi^0$ at 18.5 GeV/c †

M. J. Hones,* N. M. Cason, N. N. Biswas, J. A. Helland, V. P. Kenney, J. T. McGahan,‡ J. A. Poirier, O. R. Sander, and W. D. Shephard

Department of Physics, University of Notre Dame, Notre Dame, Indiana 46556

(Received 26 March 1970)

The reaction $\pi^+ p \rightarrow p\pi^+\pi^+\pi^-\pi^0$ has been studied at an incident π^+ momentum of 18.5 GeV/c. This reaction is dominated by strong resonance production and low four-momentum transfer squared from the target to the outgoing proton. A large excess of events in the $\pi^+\pi^+\pi^-\pi^0$ effective-mass distribution in the region from 1.52 to 2.32 GeV is observed. This enhancement is attributed primarily to $p\rho^+\rho^0$ and $pA\pi$ final states. A study of angular distributions in the $p\rho^+\rho^0$ final state suggests the importance of a double-peripheral production mechanism for these events.

I. INTRODUCTION

IN recent years there has been much interest in the production of bosons in high-energy pion-nucleon interactions. The experiment which will be discussed in this paper is a high-energy study of the reaction

$$\pi^+ p \rightarrow p\pi^+\pi^+\pi^-\pi^0. \quad (1)$$

The π^+ incident momentum was 18.5 GeV/c, the highest π^+ momentum that could be obtained at the time the experiment was run.

In Sec. II we discuss the separation of reaction (1) from other channels in the four-prong final state and in Sec. III we discuss the cross section of the reaction as well as its general features. In Sec. IV the properties of the 4π effective-mass distribution are examined. Section V deals with the properties of the $p\rho^+\rho^0$ final state.

II. EXPERIMENTAL PROCEDURES

The rf separator technique[1] was used to obtain a π^+ beam with a momentum of 18.46 GeV/c and a spread of 0.09 GeV/c from the alternating gradient synchrotron at the Brookhaven National Laboratory. The data were obtained in two separate runs using the 80-in. liquid-hydrogen bubble chamber. In first run, about 50 000 stereo triads were obtained. In the second run, about 102 000 stereo triads were obtained to give a total of 152 000 photographs.

The film was scanned for interactions (hereafter referred to as four-prong) in which four charged particles were produced at the interaction vertex. In the first part of the experiment, a fiducial region 100 cm in length was used and in the second part a region 110 cm in length was used. An increased scanning volume was possible because of the removal of lead plates from the bubble chamber.

The four-prong events were measured on an image-plane measuring machine and on three film-plane measuring machines. Approximately 57 000 four-prong events were measured. They were processed with the geometry program HGEOM[2] and kinematically fitted using the CERN program GRIND.[3] The two reactions which were kinematically fitted in addition to reaction (1) were

$$\pi^+ p \rightarrow p\pi^+\pi^+\pi^- \quad (2)$$

and

$$\pi^+ p \rightarrow n\pi^+\pi^+\pi^+\pi^-. \quad (3)$$

* Present address: Physics Department, Villanova University, Villanova, Pa. Submitted in partial fulfillment of the requirements for the Ph.D. degree, University of Notre Dame.

‡ Present address: General Research Corporation, Arlington, Va.

[1] H. W. J. Foelsche, H. Hahn, H. J. Halama, J. Lach, T. Ludlam, and J. Sandweiss, Rev. Sci. Instr. **38**, 879 (1967).

[2] J. W. Burren and J. Sparrow, Rutherford High Energy Laboratory Report No. NIR L/R/14, 1963 (unpublished).

[3] R. Bock, CERN Internal Report No. DD/EXP/62/10, 1962 (unpublished); CERN T C Program Library (unpublished).